Proof of concept of an upscaled photocatalytic multi-tube reactor : a combined modelling and experimental study

Proof of concept of an upscaled photocatalytic multi-tube reactor: a combined modelling and experimental study

Jeroen van Walsem[†], Jelle Roegiers[†], Bart Modde[§], Silvia Lenaerts[†], Siegfried Denys[†,]*

† Sustainable Energy, Air & Water Technology, Department of Bioscience Engineering, University of Antwerp, Groenenborgerlaan 171, B-2020 Antwerp, Belgium.

§ Vento Ltd., Bedrijvenpark Coupure 5, B-9700 Oudenaarde, Belgium.

* E-mail: Siegfried.Denys@uantwerp.be

Fax: +32 3 265 32 25. Tel: +32 3 265 32 30.

Keywords

Airtight chamber / HVAC / Photocatalysis / Prototype / VOC

Highlights

- Insights in upscaled reactors were acquired using a modelling approach
- A final reactor design was converted into a prototype
- The prototype was experimentally validated according the CEN-EN-16846-1
- No by-product formation was detected at realistic indoor air concentrations

Abstract

Three upscaled multi-tube photocatalytic reactors designed for integration into HVAC (Heating, Ventilation and Air Conditioning) systems were proposed and evaluated using a CFD modelling approach, with emphasis on the flow, irradiation and concentration distribution in the reactor and hence, photocatalytic performance. Based on the obtained insights, the best

reactor design was selected, further characterized and improved by an additional proof of concept study and eventually converted into practice. Subsequently, the scaled-up prototype was experimentally tested according to the CEN-EN-16846-1 standard (2017) for volatile organic compound (VOC) removal by an external scientific research center. The combined modelling and experimental approach used in this work, leads to essential insights into the design and assessment of photocatalytic reactors. Therefore, this study provides an essential step towards the optimization and commercialization of photocatalytic reactors for HVAC applications.

Graphical abstract

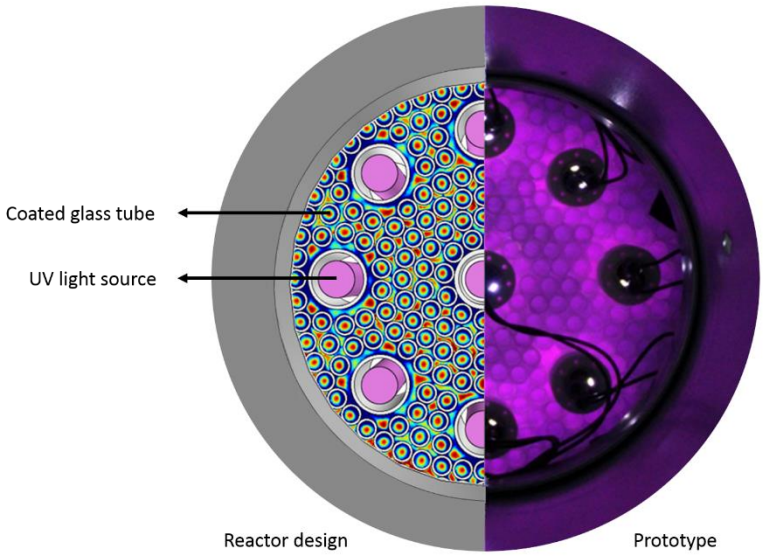

1. Introduction

During the last decades, photocatalysis has been extensively studied as a remediation for indoor and outdoor air pollution. To this day, however, successful applications of photocatalysis have been restricted to the field of self-cleaning surfaces and coatings [1,2]. Nevertheless, a great deal of literature has been devoted to designing photocatalytic systems to address indoor air pollution, but the research usually only goes as far as the development of laboratory scale reactors and devices [3–6].

Modelling is often proposed as a promising method to speed up the process towards commercial valorization. Although modelling the photocatalytic process is very challenging due to the combined occurrence of different physical and chemical phenomena, several models have been proposed that can accurately predict the performance of a photocatalytic reactor for different realistic operating conditions [7–9]. The latter implies the use of numerical methods. As shown in previous work and the literature [10–13], analytical methods are very useful for obtaining results quickly, but are restricted to simple geometric designs of photocatalytic devices, while numerical methods usually require a considerably longer simulation time, but are more widely applicable and better suited to study more complex systems. In addition, numerical model simulations have led to new insights into how a photocatalytic device can be optimized to achieve better reactor efficiency [14]. The main challenge is to simultaneously meet the different criteria for efficient design: complete mineralization of VOCs at ppb levels, high UV irradiation on the active surfaces with a minimum of energy consumption, low pressure drop, an efficient photocatalyst and no formation of harmful by-products [7].

In our previous work we presented borosilicate glass tubes as a suitable substrate for HVAC applications[14–16]. Glass tubes can easily be coated and stacked to constitute a transparent monolithic ‘multi-tube reactor’. The main advantages in terms of pressure drop and exposed photocatalytic surface area were emphasized and a high efficiency with respect to the degradation of acetaldehyde in air was demonstrated. Subsequently, a profound characterization of lab-scale multi-tube reactors showed that a trade-off between photocatalytic activity and UV-A light transmission should be considered. By increasing the coating layer thickness, a higher photocatalytic activity is reported. However, the UV-A light transparency of the layer decreases accordingly, resulting in a drastic reduction of light irradiance throughout the entire reactor. Therefore, an optimized configuration of the light sources is of the utmost importance for upscaled photocatalytic reactors.

In this work we present a modelling approach to evaluate and compare a few upscaled, virtual prototypes, based on the concept of multi-tube reactors. Three different designs were studied, which differed in terms of the configuration of light sources used. Based on the obtained insights gained from the preliminary modelling study, we made a selection of the best performing reactor and performed a proof of concept. The final design was built and its performance was tested according to the CEN-EN-16846-1 standard for VOC removal (2017). For the future assessment of photocatalytic prototypes towards commercialization, there is an urgent need for upgraded standards concerning large pilot scale experiments [17,18].

2. Methodology

2.1 A brief overview of the modelling approach

A modelling approach was used to evaluate the flow inside the reactor, irradiation on the catalytic surfaces, pollutant concentration and the photocatalytic performance of the different reactor configurations. A thorough feasibility study of the lab-scaled multi-tube reactor with respect to photocatalytic coating and substrate selection, light permeability and pressure losses of the system, is described in van Walsem et al. (2018) [16]. The commercial software package Comsol Multiphysics v.5.4 was used to perform all numerical simulations. For a detailed description of the modelling approach, the reader is referred to our previously published work [14,15,19]. In short, for all models a user-defined mesh was created with an average mesh quality of 0.673, which is a dimensionless quantity between 0 and 1, where 1 represents a perfectly regular element, in the chosen quality measure, and 0 represents a degenerated element. The air flow direction is parallel to the length of the coated glass tubes and therefore it was possible to reduce the number of mesh elements by using triangular prism-shaped elements in the photocatalytic active part of the geometry.

To create a sufficiently fine mesh for the different geometries, 1.8 x 10^6 to 2.7 x 10^6 prism-shaped elements was needed. When simulating the acetaldehyde transport through the multi-tube reactor, a large local gradient was expected between bulk concentrations and concentrations close to the catalytic surface. This is valid for high photocatalytic reaction yields. Hence, 4 boundary layers were added to the inner catalytic surfaces of the glass tubes. The cylindrical emission of the fluorescent light sources were represented by a curved surface with rectangular boundary elements. The remaining parts of the geometry were meshed with tetrahedral elements.

A key factor in the optimization procedure is the distribution of UV light in the reactor and the uniformity of the irradiance on the photocatalytic surfaces. In previous work, a radiation field model was developed in Comsol Multiphysics, in which light is represented as rays, departing from the lamp surface [14]. The full details on the radiation field model are described in Roegiers et al. (2017) [14]. The rays propagate through the system and interact with the coated glass tubes through refraction and absorption. The governing equations to solve are ray trajectories given by (Eq. 1):

$$\begin{cases} \dfrac{d\boldsymbol{k}}{dt} = -\dfrac{\partial \omega}{\partial \boldsymbol{q}} \\ \dfrac{d\boldsymbol{q}}{dt} = \dfrac{\partial \omega}{\partial \boldsymbol{k}} \\ \omega = \dfrac{c|\boldsymbol{k}|}{n(\boldsymbol{q})} \end{cases} \quad 1$$

with $\boldsymbol{k}$ the wave vector, ω the angular frequency, c the speed of light in vacuum, n the real part of the refractive index and $\boldsymbol{q}$ the position vector. Attenuation of UV light at the photocatalytic surface is controlled by the imaginary part of the refractive index and the thickness of the coating, both related to the loading of P25 in the sol-gel coating [14,20]. Consequently, irradiance can be coupled to reaction kinetics, as further explained.

A k-ε-turbulent air flow model was used to model the airflow through the reactor [21]. In each modelled case, a volumetric flow rate at the inlet and a constant atmospheric pressure at the outlet were specified. A steady-state solution was generated by solving the governing equations of momentum and mass continuity with a direct stationary solver (Eq. 2-3):

$$\rho(\mathbf{u}\cdot\nabla)\mathbf{u} = \nabla\cdot\left(-p\mathbf{I} + (\mu+\mu_T)(\nabla\mathbf{u} + (\nabla\mathbf{u})^T)\right) \quad 2$$

$$\rho\nabla(\mathbf{u}) = 0 \quad 3$$

With ρ the air density (1.2044 kg m^{-3}) [22], $\mathbf{u}$ the velocity vector (m s^{-1}), $\mathbf{I}$ an identity matrix, p the pressure (Pa), μ the dynamic viscosity (Pa·s) and μ_T the eddy viscosity (Pa·s), which is calculated by the k-ε-model for a turbulent flow. A no slip condition was applied to the reactor walls. The transport of acetaldehyde through the reactor was solved with the convection-diffusion equation, by coupling the velocity field of the previous stationary study (Eq. 4):

$$\nabla\cdot\left(-D\nabla C_{CH_3CHO}\right) + \mathbf{u}\cdot\nabla C_{CH_3CHO} = 0 \quad 4$$

With D the diffusion coefficient of acetaldehyde in air (1.25 x 10^{-5} m² s^{-1}) [10], C_{CH_3CHO} the bulk concentration of acetaldehyde (mol m^{-3}) and $\mathbf{u}$ the velocity field vector (m s^{-1}).

To simulate simultaneous adsorption, desorption and reaction at the surface of the tubes, a new species CH_3CHO_{ads} was introduced, with a corresponding surface concentration $C_{CH_3CHO,ads}$ (mol m^{-2}). Adsorption and desorption phenomena were modelled as a flux from the bulk acetaldehyde towards the coated glass tubes (Eq. 5):

$$-\boldsymbol{n}\cdot\left(-\mathrm{D}\nabla C_{CH_3CHO}\right) = -R_{ads} + R_{des} \quad 5$$

With $\mathbf{n}$ the normal vector of the boundary pointing towards the bulk phase. R_{ads} and R_{des} are the species fluxes towards and outwards the boundary respectively, given by the Langmuir expressions (Eq. 6-7):

$$R_{ads} = k_{ads} C_{CH_3CHO} \left(1 - \frac{C_{CH_3CHO,ads}}{\Gamma_s}\right) \quad 6$$

$$R_{des} = k_{des} \frac{C_{CH_3CHO,ads.}}{\Gamma_s} \quad 7$$

With k_{ads} the adsorption rate constant (m s^{-1}), k_{des} the desorption rate constant (mol m^{-2} s^{-1}) and Γ_s the maximum surface concentration, corresponding to full occupation of active sites, as determined in previous research for the P25 loaded sol-gel coatings (mol m^{-2}) [16]. The photocatalytic elimination of acetaldehyde is described by an additional sink term R_{pco} (Eq. 8):

$$\frac{\partial C_{CH_3CHO,ads}}{\partial t} = R_{ads} - R_{des} - R_{pco} \quad 8$$

With R_{pco} the photocatalytic reaction rate (mol m^{-2} s^{-1}). The latter can be further expressed as a first order reaction rate (Eq. 9):

$$R_{pco} = k_{pco}(I)\, C_{CH_3CHO,ads} \quad 9$$

Where $k_{pco}(I)$ represents the irradiance dependent photocatalytic reaction rate constant (1 s^{-1}). In the literature, the following equation (Eq. 10) was proposed for the reaction rate constant $k_{pco}(I)$ [23–25]

$$k_{pco}(I) = \begin{cases} k_0 I & , I < 10\ W/m^2 \\ k_0\sqrt{I_0 \cdot I} & , I > 10\ W/m^2 \end{cases} \quad 10$$

With k_0 an empirical constant [m^2 W^{-1} s^{-1}] for $I < I_0$ the threshold of 10 W m^{-2} and I (W m^{-2}) the irradiance, as derived from the radiation field model. The full details on intrinsic kinetic parameter estimation and reaction kinetics are described in van Walsem et al. (2016) & Roegiers et al. (2017) [14,15]. All relevant (kinetic) parameters of the tested coatings, as determined in previously published work, are summarized in Table 1 [14].

Table 1: Intrinsic parameters of the sol-gel coatings [14]

Parameter	10 g L^{-1} P25	30 g L^{-1} P25
k_{ads} [m s^{-1}]	2.02×10^{-3}	2.02×10^{-3}
k_{des} [mol m^{-2} s^{-1}]	2.30×10^{-7}	2.30×10^{-7}
k_0 [m^2 W^{-1} s^{-1}]	8.52×10^{-4}	8.52×10^{-4}
Γ_s [mol m^{-2}]	7.78×10^{-5}	1.28×10^{-4}
$Coating\ thickness\ [nm]$	370	500

2.2 A preliminary reactor design study using a modelling approach

Three virtual reactor designs were considered to provide insight into the photocatalytic performance of real-scale multi-tube reactors for HVAC applications. The general design was based on a standard diameter of commonly used ventilation ducts, i.e. 16 cm. The total length of the reactor, consisting of coated glass tubes, was set at 30 cm, of which a middle section of 20 cm was occupied by glass tubes (Figure 1). The coated glass tubes have an inner diameter of 7 mm and an outer diameter of 9 mm (7ID9ED), as previously optimized in terms of pressure drop and exposed photocatalytic surface area [16]. A 10 g L^{-1} P25 based powder-modified sol-gel, proposed by Chen *et al.* (2006), was considered in the virtual designs [26]. For this P25 loading an optimal result was obtained in previous work for multi-tube reactors, in terms of photocatalytic activity and transparency [16]. As light sources, T5 fluorescent UV-A light sources (Sylvania F8W/BLB) were simulated within the reactor device. Three different configurations of UV-A light sources were proposed for the general reactor design, as shown in Figure 1.

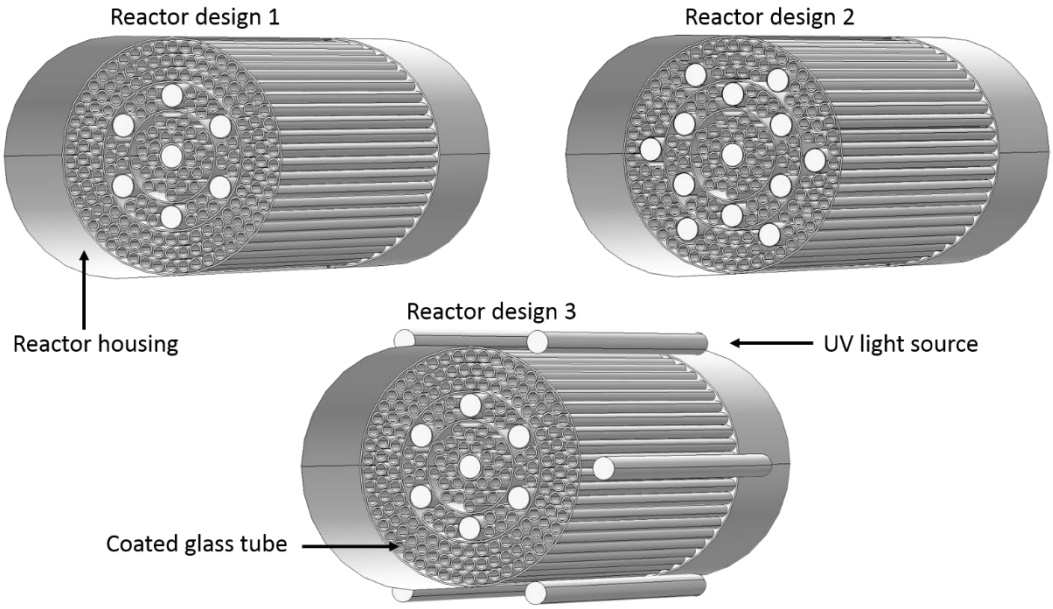

Figure 1: Proposed reactor designs characterized by an internal diameter of 16 cm, a variable number of T5 fluorescent light sources and filled with 7ID9ED coated glass tubes.

Design 1 contained 191 coated 7ID9ED tubes and 7 UV-A sources, positioned in the reactor. In design 2, 161 coated 7ID9ED tubes were used and 13 UV-A sources, all of which were positioned within the reactor housing. Finally, design 3 contained 191 coated 7ID9ED tubes, 7 UV-A sources placed inside the reactor housing, and 6 sources placed outside the housing (Figure 1).

2.3 Proof of concept reactor design: model-based evaluation

Based on the insights gained with respect to the light source configuration from the abovementioned design study, a more practical design for the reactor was proposed and evaluated by means of an additional modelling study. In this design the reactor length was reduced from 30 to 24 cm to match the standard length of the fluorescent UV sources. To compensate for the reduced reactor length, the diameter of the reactor was increased from 16 to 20 cm to provide more photocatalytic surface (Figure 2a). By increasing the reactor diameter, we could also accommodate for the mass transfer limiting process (discussed in the results

section) by reducing the flow velocity within the tubes. In total, 9 well-positioned fluorescent UV sources were used to ensure uniform light distribution in the reactor and to obtain at least an irradiation of 1 W m^{-2} on the surfaces of the glass tubes. For the same reason, all UV sources were positioned inside the reactor housing and the number of glass tube layers between the UV sources and the reactor housing was limited to 2. Both these design considerations were based on the findings of the abovementioned study as discussed in the results section. In addition, uncoated borosilicate glass tubes (internal diameter of 23 mm and an external diameter of 25 mm) were placed around the UV sources such that the air flow through these tubes could cool the UV sources in a practical device.

Before assembling the final reactor design, the possibility of using two different coatings and two different UV-light sources was tested. A 10 g L^{-1} and 30 g L^{-1} P25 loaded sol-gel coatings were considered, both of which had a high removal capacity of acetaldehyde, as described in earlier work [16]. In addition, the influence of the UV-A irradiation on the photocatalytic performance was studied by replacing the Sylvania F8W/BLB T5 lamps (170 W m^{-2}) by Philips BL TL8W BLB lamps, resulting in a lower irradiation, i.e. 140 W m^{-2}, as measured by a calibrated Avantes Avaspec-3648 spectrometer.

2.4 Proof of concept reactor design: experimental evaluation

The final reactor design was converted into a prototype. Figure 2 shows a picture of the assembled system with relevant sizes. The reactor housing (20 cm diameter) was made of galvanized steel, since this is the most used material for the manufacture of air ducts. Conically shaped diffusers, also made of galvanized steel, were attached to connect the reactor to standardized ventilation ducts with a diameter of 16 cm. All fluorescent UV light sources (in this case the best performing lamps, i.e. Sylvania F8W/BLB T5) were individually connected to an electronic ballast (Vossloh Schwabe type ELXs 116.900). A fan (Wallair W-style 230V; 15 cm diameter; 290 m^3 h^{-1}) was used to generate a realistic airflow during the photocatalytic

experiments. Note that in an HVAC system this fan is not required since the reactor concept is optimized in terms of pressure losses and thus is able to operate with the fan of the ventilation system [16].

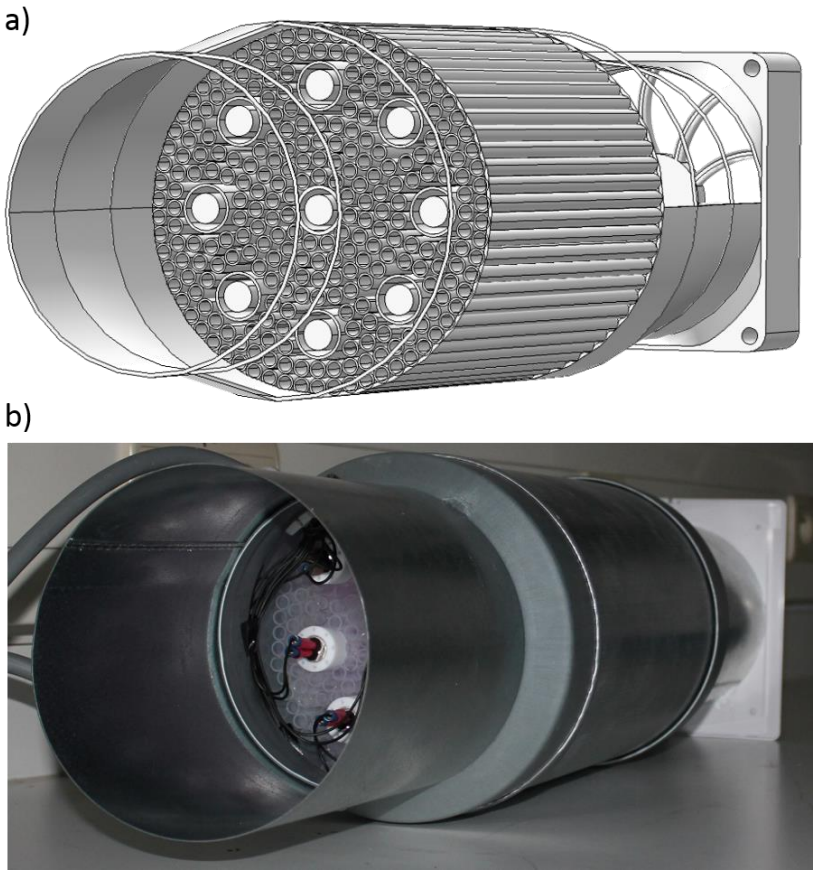

Figure 2: (a) Final design of the proof of concept reactor converted into a (b) prototype, characterized by an internal diameter of 20 cm, 9 T5 fluorescent light sources and filled with 7ID9ED coated glass tubes.

The constructed prototype was then evaluated according to the CEN-EN-16846-1 standard for VOC removal by the CERTECH research center (Seneffe, Belgium). For a detailed description of the methodology, the reader is referred to the abovementioned standard. In short, the tests were carried out in an airtight climate chamber of 1.2 m^3. A fan was installed in the chamber to ensure a uniform dispersion of the compounds. VOCs and CO_2 were measured online with an ion molecule reaction-mass spectrometer (IMR-MS), a μ-GC and a chemiluminescence NOx analyzer, respectively. The experiments were carried out at an temperature of 22 ± 3°C and a

relative humidity of 50 ± 5%. Prior to each experiment, the climate chamber was purged with clean humid air during 24 hours with the reactor switched on. Eventually, the prototype was switched off and the compounds were introduced in the chamber via a syringe. After achieving a stable concentration for all compounds, the prototype was switched on to initiate the photocatalytic reactions. To quantify possible by-product formation, a total of four air samples were taken for 15 minutes on 2,4-Dinitrophenylhydrazine (DNPH) and Airtoxics cartridges (Camsco, Inc), i.e. before introduction of the VOCs (T0), right after introduction of VOCs (T1), halfway (T2) and at end of the experiment (T3). The Airtoxics cartridges were thermally desorbed and analyzed online by a GC-MS. The DNPH samples were chemically desorbed and analyzed with a high-performance liquid chromatograph (HPLC). Two experiments were carried out in the climate chamber, in which the photocatalytic degradation was examined of (1) a mixture of VOCs in the ppbv range to study the efficiency of the prototype and (2) a mixture of VOCs in the ppmv range to study the VOC mineralization towards CO_2. The first experiment consists of three cycles where each time VOCs are introduced in the chamber via a syringe. The introduction of these VOCs is not completely reproducible whereby the initial concentrations of VOCs slightly differ for each cycle.

3. Results and discussion

3.1 A preliminary reactor design study using a modelling approach

3.1.1 Flow, irradiation and concentration distribution

A modelling approach was used to obtain insights in the flow, irradiation and concentration distribution and consequently the photocatalytic performance of the reactor designs. The purpose of this section is to study the single pass removal capacity in relation to different light source configurations. As the final objective is to create an applicable prototype, it is important to gain insights in the trade-off between energy consumption and removal capacity. Figure 3

shows the distribution of the flow velocity for the three proposed designs with a length of 30 cm, on a cross section halfway the reactor. A velocity of 3 m s^{-1} at the entrance of the reactor, i.e. a typical flow rate in HVAC systems, results in approximately a doubling of the flow velocity in the individual glass tubes. As can be seen in the figure, there is a big difference between the airflow velocity within the glass tubes and the velocity observed in the interstices between the tubes. Obviously, the flow distributions of designs 1 and 3 are identical since they do not differ in terms of number and position of the glass tubes as can be seen in Figure 3 and thus the volumetric flux through each tube remains the same. The flow velocity through the glass tubes in design 2 is slightly higher, but still results in a minimum pressure drop of about 55 Pa, as evidenced in Figure 4.

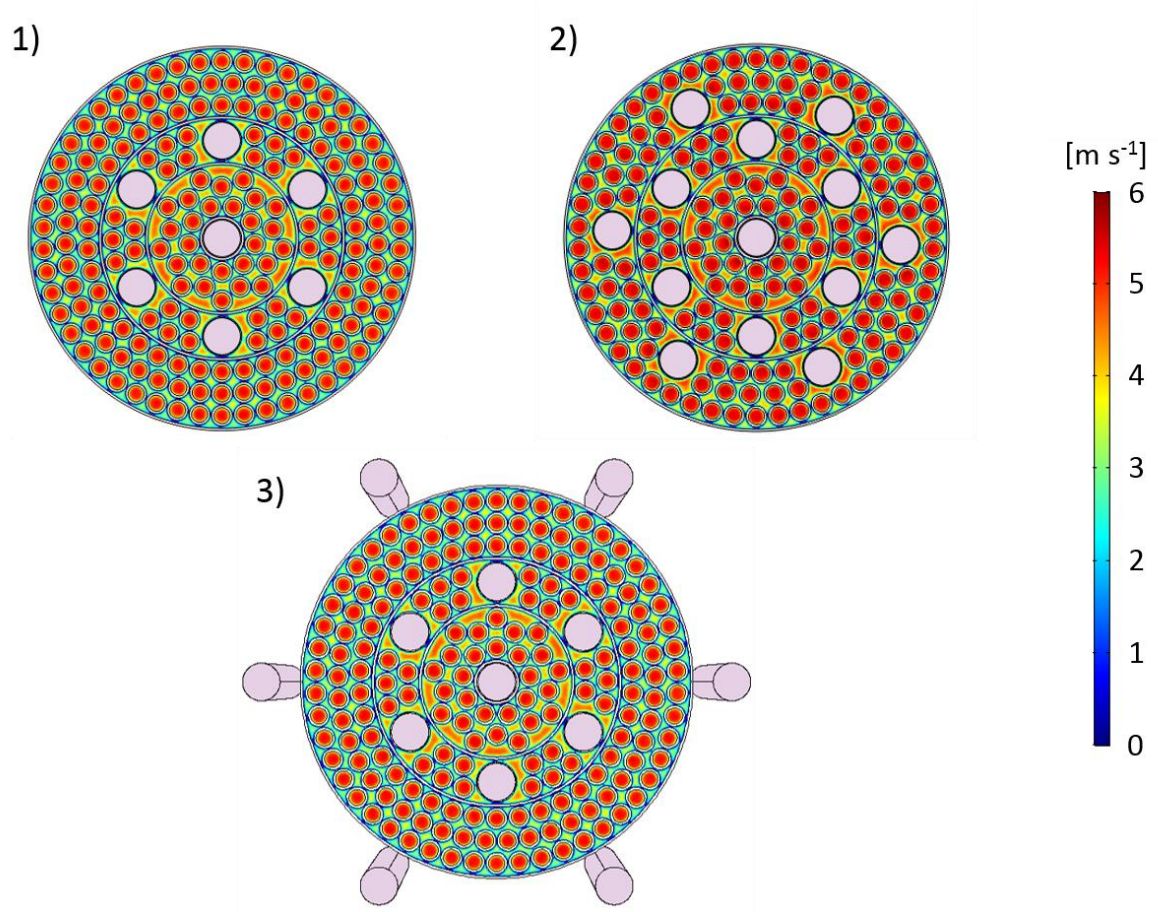

Figure 3: Distribution of the flow velocity for the 3 proposed reactor designs (for an inlet flow rate of 3 m s^{-1})

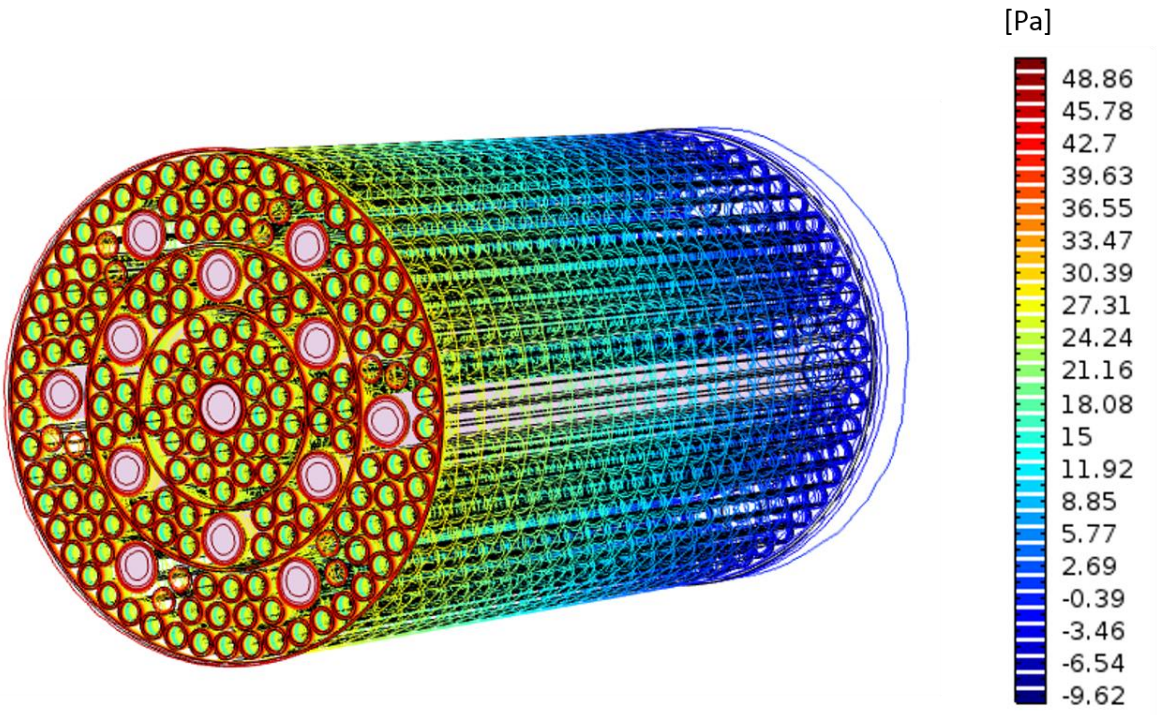

Figure 4: The pressure drop in design 2 for an inlet flow rate of 3 m s^{-1} [Pa]

Figure 5 shows the distribution of the irradiation on the coated surfaces for the three proposed designs, on a log scale. Unfortunately, there is no clear answer to the question which minimum level of irradiation is required for a reasonably working photocatalytic system. In general, the lower the irradiation, the lower the chance that a photocatalytic reaction occurs [27–30]. An important criterion of a prototype for this specific application is a minimal operational cost, therefore we specifically minimized the energy consumption. We decided to set the lower limit of irradiation for the prototype to 1 W m^{-2}, which corresponds to 0 on the log scale. As can be seen from Figure 5, the irradiation quickly extinguishes in the reactor. It is clear that a third row of glass tubes, with respect to the nearest UV light source, receives an insufficient level of irradiation, as indicated by the bluish colors. As indicated on Figure 6 (design 1), the acetaldehyde concentration remains unchanged in the outer row of glass tubes corresponding to irradiation levels lower than 1 W m^{-2}. The most uniform irradiation pattern is observed in design 3. However, by placing fluorescent UV light sources outside of the reactor, a substantial portion of the emitted radiation will not be able to reach the photocatalytic surfaces of the glass

tubes. This can possibly be solved by placing a reflective casing around the reactor, which is, however, undesirable for the compactness of the device. The irradiation pattern in design 2 is less uniform, but this configuration has a more efficient use of radiative power. Design 1 lacks uniformity and is unable to provide all photocatalytic surfaces with a sufficient amount of irradiation due to the poor placement and/or the insufficient amount of UV light sources.

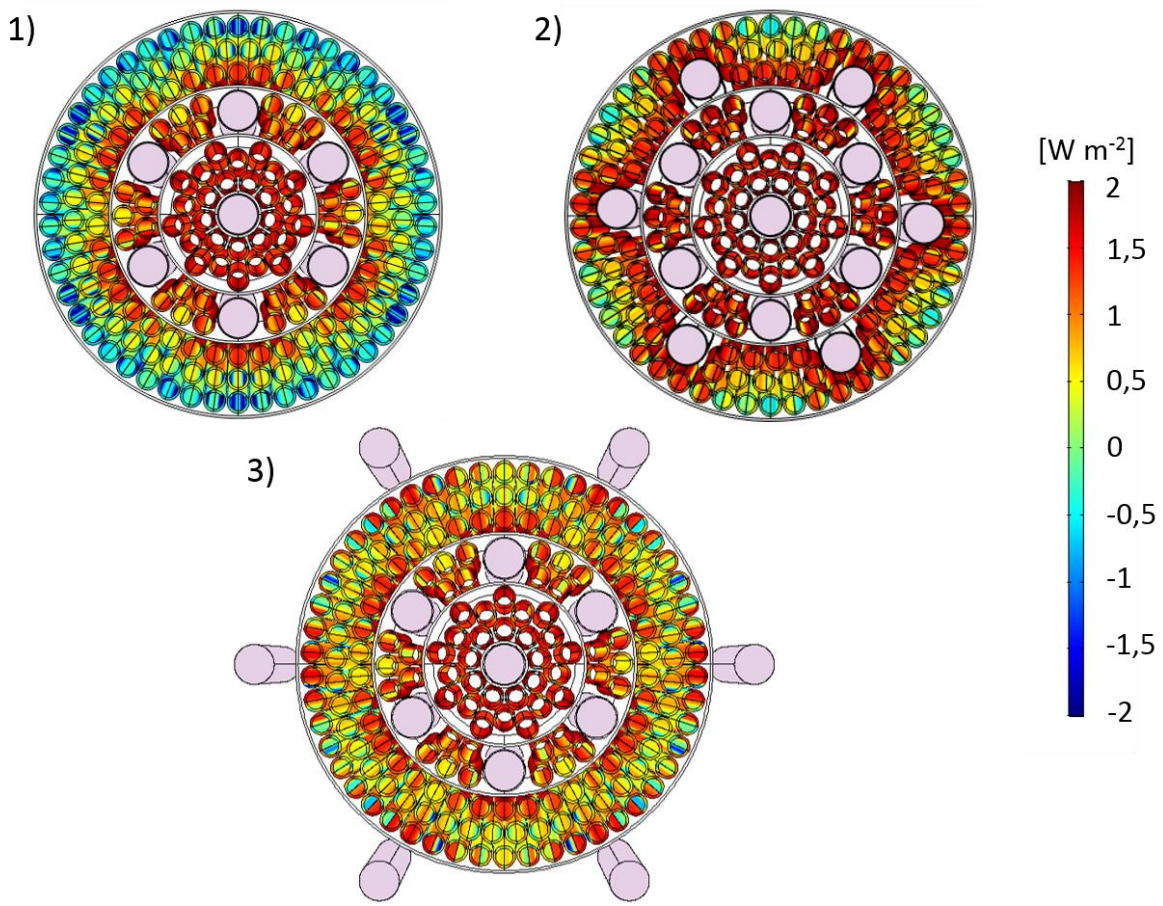

Figure 5: The irradiation distribution in 3 proposed designs (log scale) [W m^{-2}]

Figure 6 shows the local acetaldehyde concentration distribution on a cross section halfway the reactor for the 3 proposed designs, corresponding to the aforementioned flow and irradiation distributions. The previous conclusions with regard to the irradiation distribution are supported by the local concentration profiles in the proposed designs, namely (1) a negligible photocatalytic activity in the outer layers of glass tubes in design 1, due to the low irradiation

intensity; (2) a much more effective result due to an efficient use of UV sources in design 2 and (3) a relatively uniform but moderate effect in design 3.

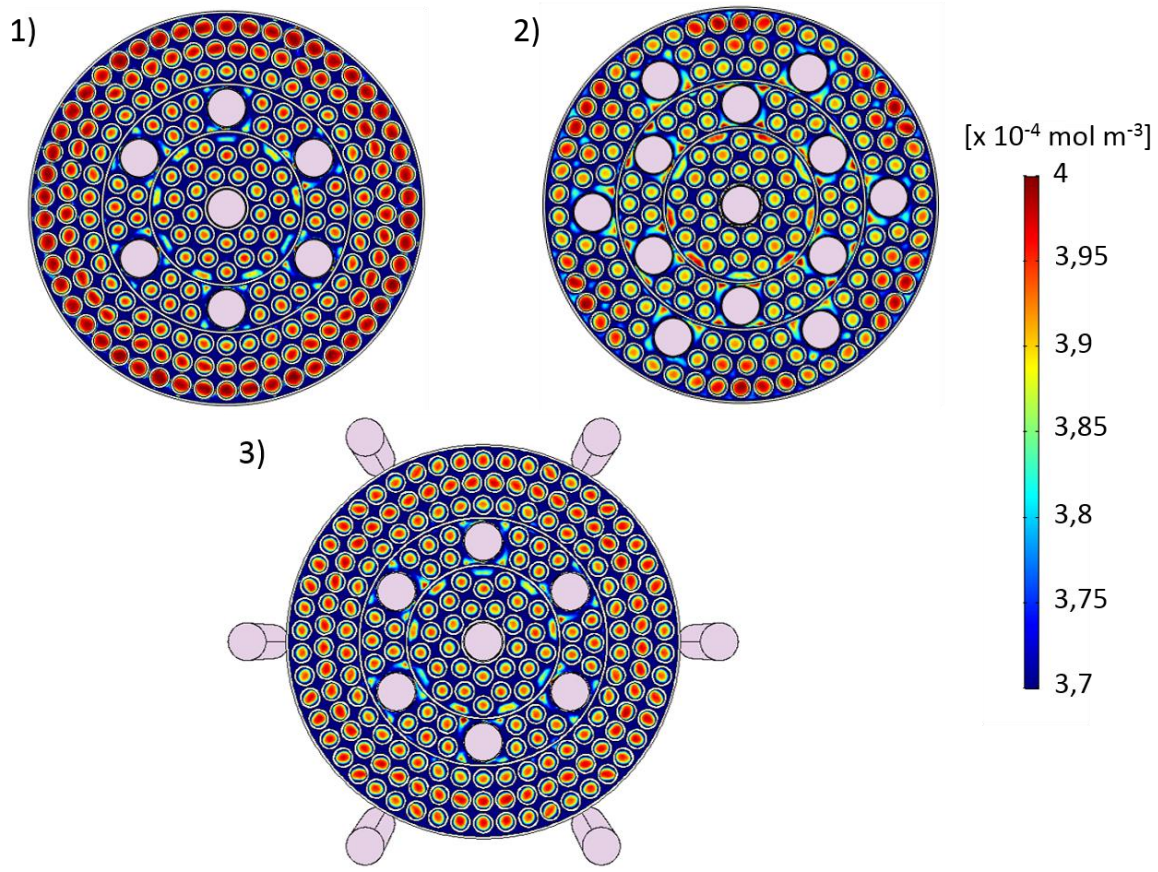

Figure 6: Acetaldehyde concentration profiles in 3 proposed designs [mol m^{-3}]

3.1.2 Photocatalytic removal capacity

A quantitative comparison of the removal capacity for acetaldehyde in a single pass through the reactor is given in Figure 7a, as calculated by the Comsol model with a relative convergence error of 1×10^{-3}. Given that the number and the position of the light sources are completely different, it is remarkable that the performance of the reactor designs are in the same order of magnitude. The latter clearly indicates that the system is controlled by mass transfer. Designs 2 and 3 perform only slightly better than design 1, even though these designs have 6 additional fluorescent UV sources positioned inside or outside the reactor. Design 2 shows the highest acetaldehyde removal capacity for the same radiation power as design 3. In this particular design, the effect of more UV sources in the reactor compensates for the disadvantage of less

photocatalytically active surface in the reactor. Figure 7b shows the capacity for removing acetaldehyde with a single pass for design 2 with two different reactor lengths: 0.3 and 1 m, i.e. 8.34 and 13.60% respectively. Apparently, tripling of the length does not imply a tripling of the acetaldehyde removal capacity. This can be explained by the mass transfer coefficient which is typically higher in the aerodynamic entrance length (where the flow is developing) of the glass tubes [22]. The entrance length L depends on the turbulent flow characteristics (the Reynolds number) and the tube diameter, as shown in Eq. 11 [31]:

$$L = 1.359\, Re^{1/4} D \qquad 11$$

According to Eq. 11 the entrance length of the glass tubes is 6.44 cm, independent of the total reactor length. A shorter reactor has a relatively longer entrance length and will therefore benefit from a higher mass transfer coefficient. Nevertheless, we want to emphasize that the entrance length also causes most of the pressure drop.

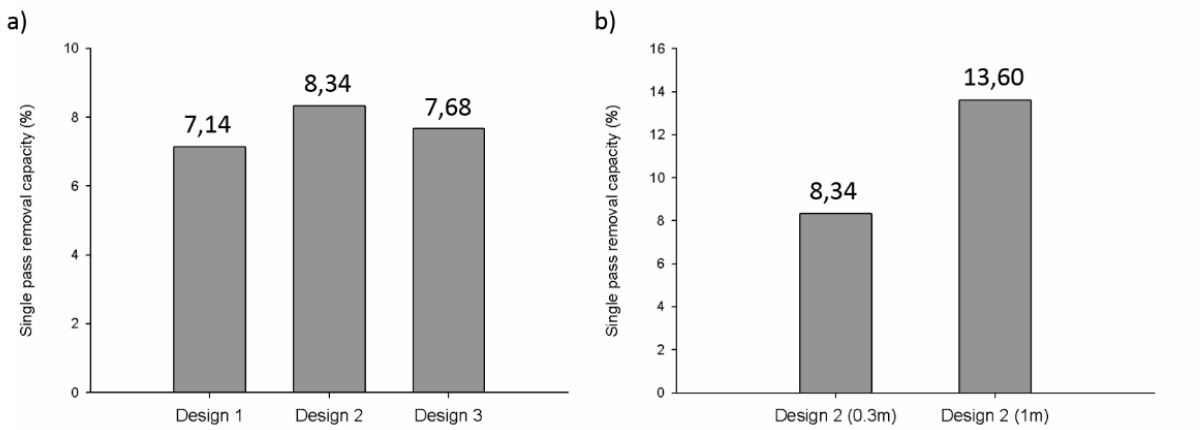

Figure 7: a) A quantitative comparison of the single pass photocatalytic acetaldehyde removal capacity and b) influence of the reactor length on the single pass photocatalytic acetaldehyde removal capacity of design 2 [%]

3.2 Proof of concept reactor design: model-based evaluation

Based on the insights obtained, an improved proof of concept reactor design is proposed, characterized by an internal diameter of 20 cm and total reactor length of 24 cm, as discussed in the methodology section. A total of 9 UV light sources were positioned in the reactor to

ensure uniform light distribution and to reach the minimum irradiation criteria of 1 W m^{-2} on the surfaces of the glass tubes, as evidenced by Figure 8.

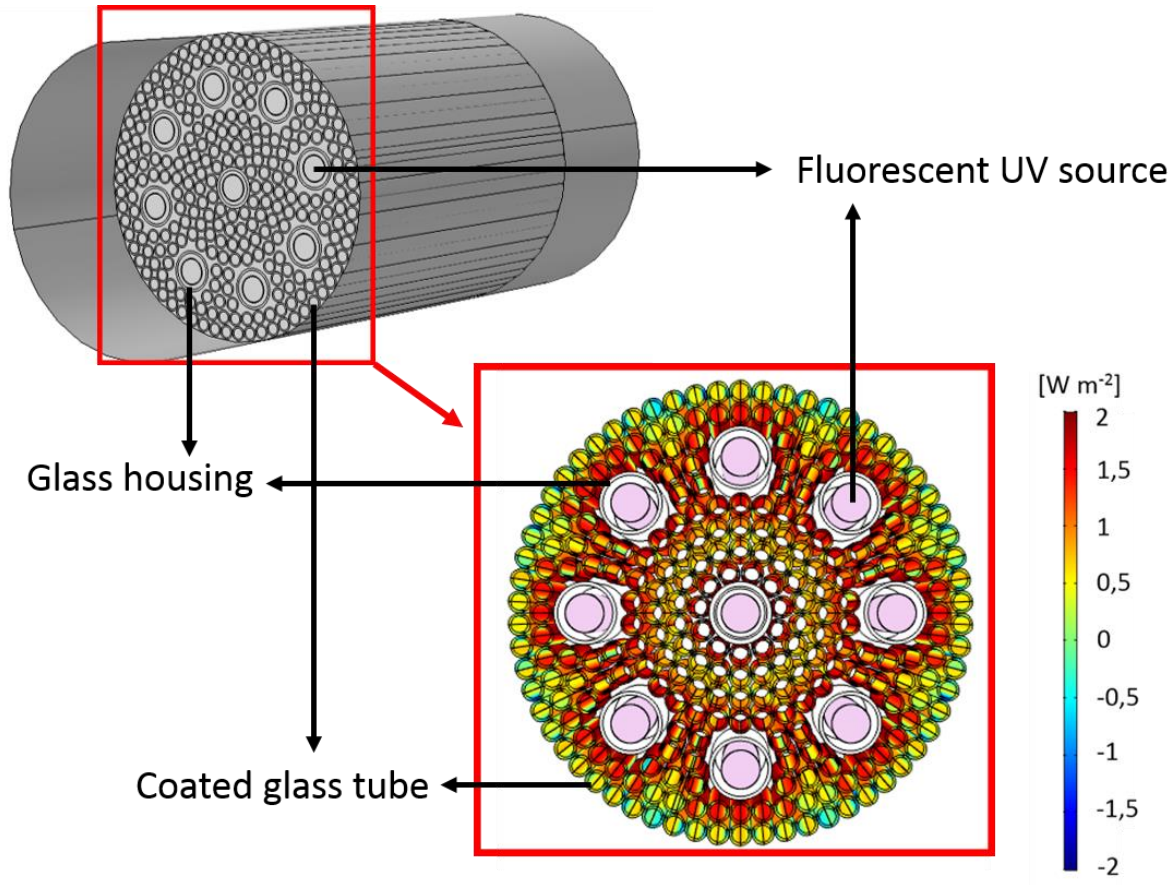

Figure 8: CFD geometry and the irradiation distribution of the proposed proof of concept reactor design (log scale) [W m^{-2}]

The effect of different P25 loaded coatings (10 g L^{-1} and 30 g L^{-1}) and irradiation conditions (Sylvania F8W/BLB T5 and Philips BL TL8W BLB UV light sources) were first tested using a modelling approach. The single-pass removal capacities of the reactor configurations are shown in Figure 9, as calculated by the Comsol model with a relative convergence error of 1×10^{-3}. The Sylvania F8W/BLB T5 lamps and Philips BL TL8W BLB lamps resulted in an irradiation of 170 W m^{-2} and 140 W m^{-2} respectively. By reducing the flow velocity, the residence time of VOCs and thus the adsorption increases, which in general has a significant positive effect on the single-pass removal capacity of the reactor, as evidenced by Figure 9. The latter reconfirms

that the system is controlled by mass transfer. Again it is emphasized that a 10 g L^{-1} coating performs best at all studied flow rates. These observations were in accordance with our previous research, where we made a thorough analysis of the effect of the coating thickness on the UV light permeability [16]. Evidently, the prototype equipped with 8W Sylvania lamps performs better than the one with 8W Philips lamps because of the more efficient conversion of power into UV radiation. However, the difference in performance is relatively small due to the mass transfer limiting process.

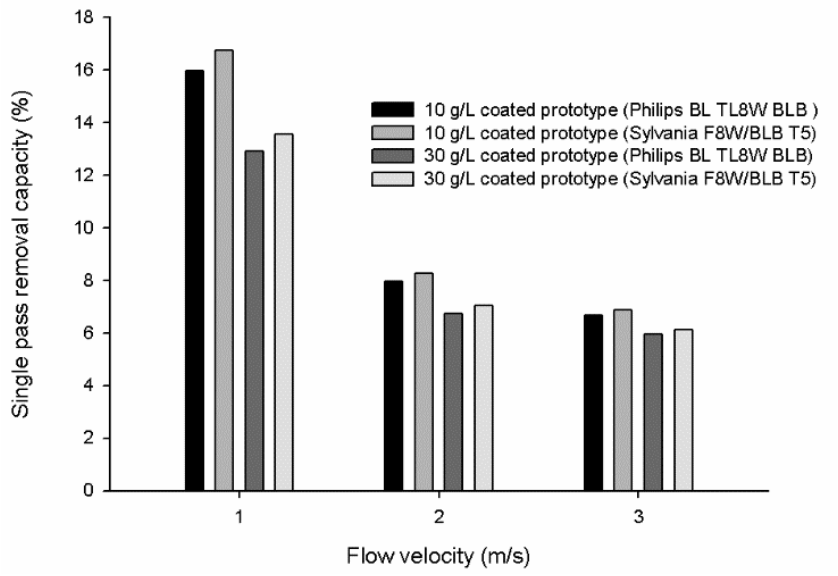

Figure 9: The single pass removal capacities of the different proof of concept reactor configurations at three different flow velocities for an inlet acetaldehyde concentration of 4 × 10^{-5} mol m^{-3} [%].

3.3 Proof of concept reactor design: experimental evaluation

In a final phase, the prototype was constructed according to the theoretical proof of concept design with Sylvania F8W/BLB T5 lamps as UV light sources (Figure 10). Consequently, the prototype was evaluated according the CEN-EN-16846-1 standard for VOC removal.

Figure 10: The proof of concept photocatalytic prototype

3.3.1 Photocatalytic experiment at concentrations in the ppbv range

A mixture of VOCs with concentrations in the ppbv range was introduced in the airtight test chamber to study the efficiency of the prototype and the by-product formation. The mixture consisted of formaldehyde, acetaldehyde, acetone, toluene and n-heptane. Figure 11 shows the evolution of the VOC concentration versus time. The experiment was performed three times in order to perform 4 DNPH and Airtoxic samplings (T0-T3) at different time frames, as indicated in Figure 11. T0 was not shown on the figure as the sampling was performed before introduction of the VOCs.

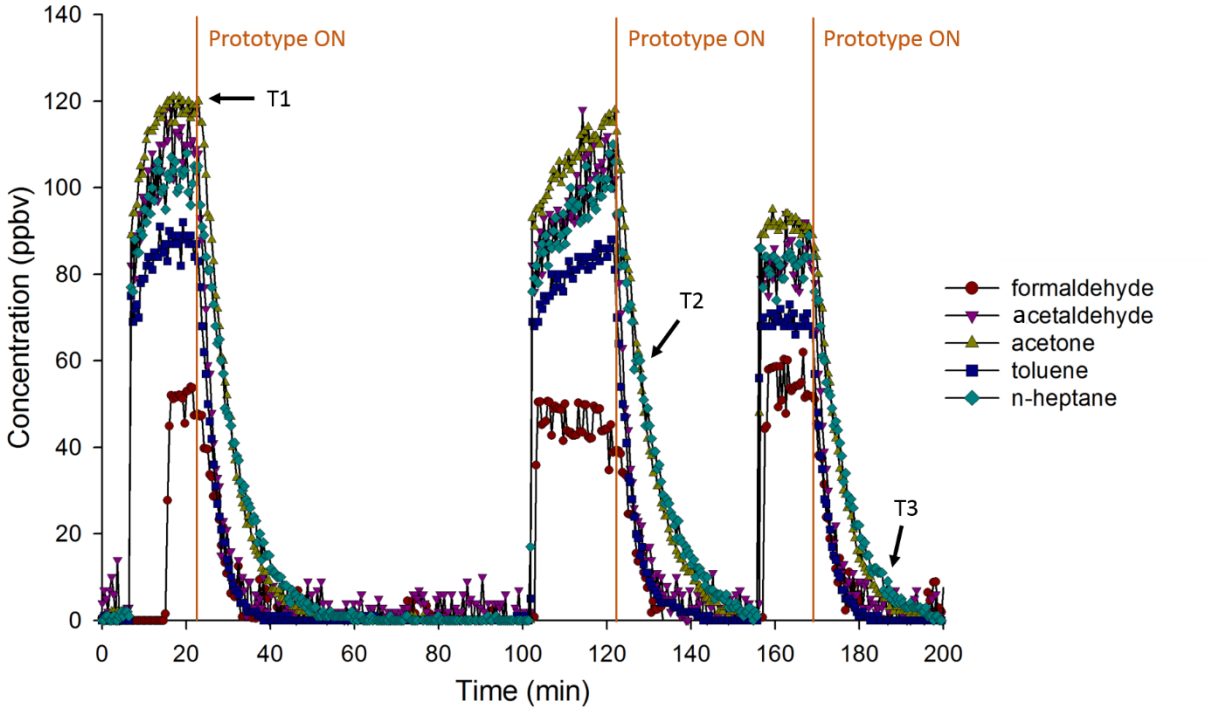

Figure 11: The evolution of the VOC concentration versus time at low (ppbv range) concentrations

The GC-MS and HPLC results on the samplings (T0-T3) are reported in Table 2. Only the introduced VOCs are detected, indicating that no secondary by-products were produced by the prototype. However, it is possible that one of the introduced VOCs is formed as a by-product when degrading another introduced VOC, e.g. formaldehyde is formed when degrading toluene. Nevertheless, in Figure 11 we can clearly observe that all introduced VOCs are continuously removed upon switching on the reactor.

Table 2: DNPH and Airtoxic cartridges analysis

DNPH analysis					
Compounds (ppbv)	**T0**	**T1**	**T2**	**T3**	**Detection limit**
formaldehyde	4	15	8	2	0.9
acetaldehyde	2	16	7	4	0.6
acetone	1	33	20	4	0.5
Air toxic cartridges analysis					

Compounds (ppbv)	T0	T1	T2	T3
acetone*	4	5	3	6
n-heptane	<0.4	25	14	0
toluene	<0.4	18	4	<0.4

*Not quantitatively adsorbed on the cartridge

According to the CEN-EN-16846-1 standard, the mixture of these 5 VOCs is regarded as a representative composition for indoor air. Hence, the total of the VOC concentrations of the first cycle of the aforementioned experiment (Figure 11) was taken as TVOC concentration, resulting in a realistic indoor concentration of 465 ppbv [32–34]. From the observed evolution of the TVOC degradation, the single-pass removal efficiency (SPRE, %) was estimated from regression, using the flow rate through the reactor and considering a perfectly mixed chamber of 1.2 m³ volume. In such case, the TVOC concentration decay in the chamber is described by the following simple equation (Eq. 12):

$$C_{TVOC}(t) = C_{TVOC,initial}\, e^{-(Q/V \cdot SPRE \cdot\, t)} \qquad 12$$

With Q the air flow (m³ s^{-1}) and V the volume of the chamber (m³). From curve-fitting of this equation with the experiment, the single-pass removal efficiency of the reactor was determined to be 7.13%. Figure 12a shows the excellent agreement of experimentally and analytically determined results, as evidenced by a coefficient of determination of 0.997. Consequently, the TVOC degradation was extrapolated to more realistic room volumes. The reactor setup, the turbulent flow regime and the flow rate were assumed to be the same in the case of a real room volume. Only the volume of the chamber changes. We assumed perfect mixed chambers, thus the geometry of the room does not affect the calculation. An example is given for a room volume of 50 m³, as shown in Figure 12b. In this case, 90% TVOC degradation is achieved in about 10 hours, considering perfectly mixed air in the room. For room volumes of 75 and 100 m³, 90% TVOC degradation is achieved in 15 and 20 hours respectively.

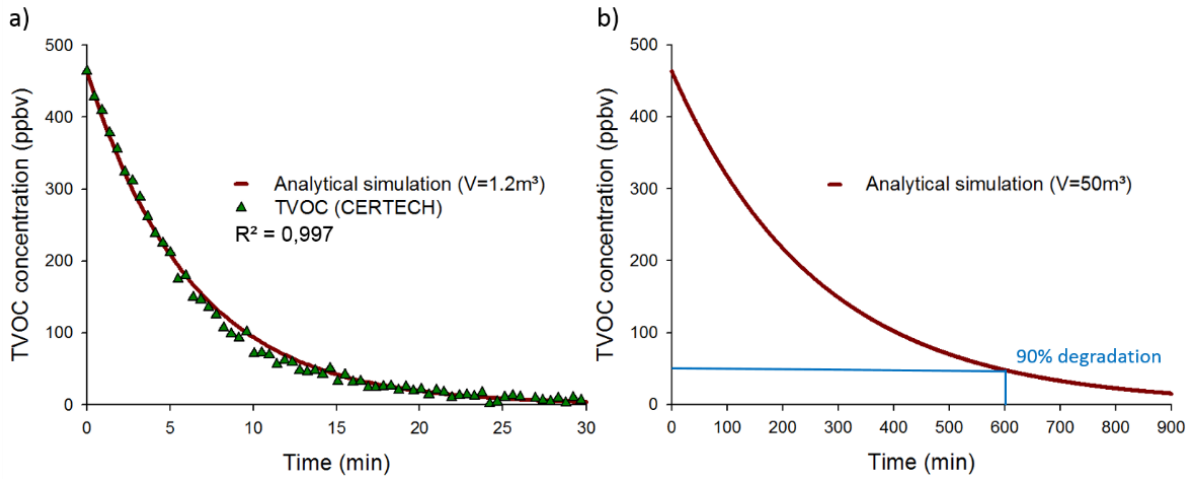

Figure 12: a) Experimental and analytically determined TVOC degradation and b) An extrapolation of the analytically determined TVOC degradation for a realistic room volume of 50 m³.

3.3.2 Mineralization study at concentrations in the ppmv range

The mineralization process was studied at ppmv range concentrations. The VOC mixture consisted of acetaldehyde, acetone, toluene and n-heptane. Formaldehyde was excluded in order to be able to detect it as a possible by-product. The concentration profiles of the VOC mixture and CO_2, as measured by the external research center CERTECH, are shown in Figure 13. The photocatalytic prototype was switched on after reaching stable concentration profiles for 15 minutes. Instantly after the prototype is turned on, a steep drop in the concentration of the introduced VOCs is observed. At the same time, CO_2 is formed, which proves the occurrence of mineralization. At the start of the photocatalytic experiment, formaldehyde was formed as the only by-product, reaching a peak concentration of 319 ppbv. The peak formaldehyde concentration represents 1.13% of the total carbon balance and was completely removed during the experiment. Based on the carbon balance, the theoretically produced CO_2 was calculated and added to Figure 13. At the end of the experiment, about 88% of the carbon originating from the VOCs was mineralized to CO_2. This appears to contradict the fact that all the introduced VOCs and potential by-products are removed from the air. The latter can be explained by the formation of strongly adsorbed species on the surface of the photocatalyst, e.g. acids

[23,24,35,36]. Unfortunately, further measurements of CO_2 versus time to control complete mineralization were not included in the CEN standard. A complete mineralization, proven by a good agreement between the theoretically calculated and experimentally formed CO_2, is expected at a later stage.

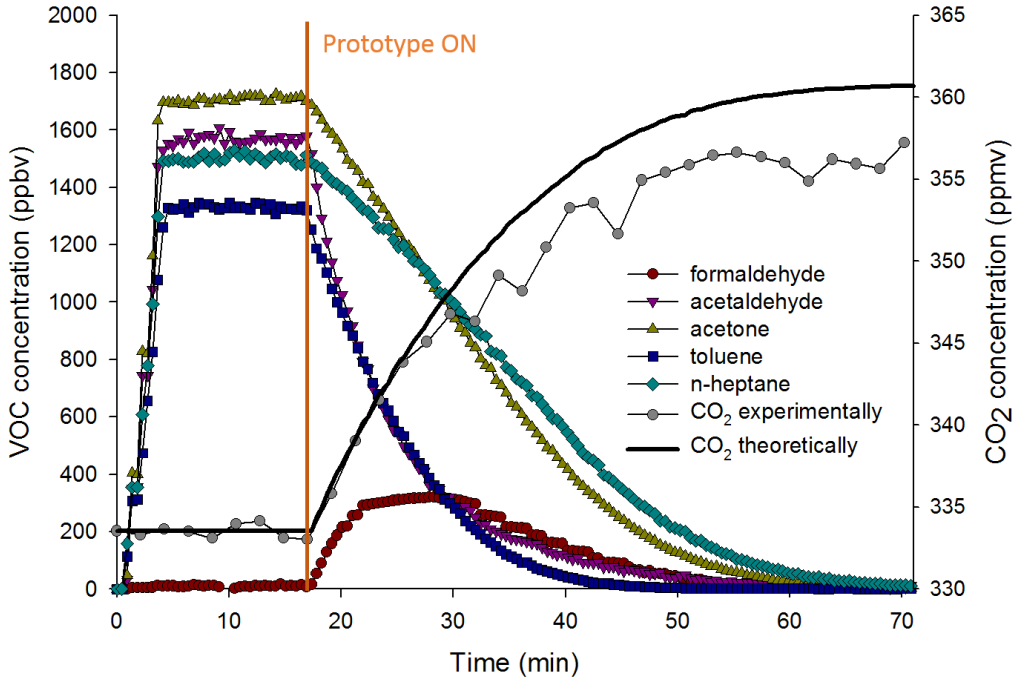

Figure 13: The concentration profiles of the VOC mixture and CO_2, as measured by CERTECH. The theoretically CO_2 production, based on the carbon balance, was added in order to quantify the mineralization rate.

4. Conclusions

Using an approach based on the combined modelling of airflow, mass transfer, irradiation and photocatalytic reactions, we could quantify the photocatalytic performance of three proposed multi-tube reactor designs. In contrast to the devices typically developed for laboratory studies where low flow rates are generally used, mass transfer proved to be the limiting step for reactor designs at high, realistic flow rates. Therefore, the number of fluorescent UV light sources used and their intensity had a limited, but not negligible, effect on the photocatalytic performance of the reactor. To solve this, an important insight was that lower air velocities for the same flow

rate and thus a higher residence time of the pollutant were favorable for the performance of the reactor. This can be accomplished by designing shorter, wider reactors. In addition, the number of coated glass tubes that are stacked in the reactor should be sufficient to provide the required photocatalytic surface in the reactor. Based on the acquired insights of the reactor design study and taking into account some practical implications, a final reactor design was suggested and evaluated by means of an additional modelling study. The theoretical proof of concept design was converted into a prototype and consequently evaluated according the CEN-EN-16846-1 standard for VOC removal by an external scientific research center 'CERTECH'. The prototype was able to eliminate all introduced VOCs at concentrations in the ppbv range without formation of by-product, as demonstrated by Airtoxics and DNPH cartridge samples. An additional experiment at concentrations in the ppmv range showed the mineralization of the VOCs. A small amount of formaldehyde was formed as the only by-product at the start of the experiment and was completely removed during the experiment. This study provides essential insights into reactor design and consequently the assessment of upscaled photocatalytic devices. However, we want to emphasize the need to carry out large-scale experiments to assess the performance of photocatalytic reactors in general and multi-tube reactors in particular. Moreover, proof of concept studies in realistic indoor air conditions can lead to further insights.

5. Acknowledgement

J.V.W. acknowledges the Agentschap Innoveren & Ondernemen for a PhD fellowship.

6. References

[1] Y. Boyjoo, H. Sun, J. Liu, V.K. Pareek, S. Wang, A review on photocatalysis for air treatment: From catalyst development to reactor design, Chem. Eng. J. 310 (2017) 537–559. doi:10.1016/j.cej.2016.06.090.

[2] Y. Paz, Application of TiO2 photocatalysis for air treatment: Patents' overview, Appl. Catal. B Environ. 99 (2010) 448–460.

[3] P. Bourgeois, E. Puzenat, L. Peruchon, F. Simonet, D. Chevalier, E. Deflin, et al., Characterization of a new photocatalytic textile for formaldehyde removal from indoor air, Appl. Catal. B Environ. 128 (2012) 171–178. doi:10.1016/j.apcatb.2012.03.033.

[4] M. Hossain, G.B. Raupp, S.O. Hay, T.N. Obee, Three-Dimensional Developing Flow Model for Photocatalytic Monolith Reactors, AICHE. 45 (1999).
[5] R. Sun, A. Nakajima, I. Watanabe, TiO2 -coated optical fiber bundles used as a photocatalytic filter for decomposition of gaseous organic compounds, J. Photochem. Photobiol. A Chem. 136 (2000) 111–116.
[6] K.H. Wang, H.H. Tsai, Y.H. Hsieh, The kinetics of photocatalytic degradation of trichloroethylene in gas phase over TiO2supported on glass bead, Appl. Catal. B Environ. (1998). doi:10.1016/S0926-3373(97)00099-4.
[7] G.B. Raupp, A. Alexiadis, M.M. Hossain, R. Changrani, First-principles modeling, scaling laws and design of structured photocatalytic oxidation reactors for air purification, Catal. Today. 69 (2001) 41–49. doi:10.1016/S0920-5861(01)00353-4.
[8] M. Mohseni, F. Taghipour, Experimental and CFD analysis of photocatalytic gas phase vinyl chloride (VC) oxidation, Chem. Eng. Sci. 59 (2004) 1601–1609. doi:10.1016/j.ces.2004.01.017.
[9] A. Queffeulou, L. Geron, E. Schaer, Prediction of photocatalytic air purifier apparatus performances with a CFD approach using experimentally determined kinetic parameters, Chem. Eng. Sci. 65 (2010) 5067–5074. doi:10.1016/j.ces.2010.05.024.
[10] S.W. Verbruggen, S. Lenaerts, S. Denys, Analytic versus CFD approach for kinetic modeling of gas phase photocatalysis Analyθc, Chem. Eng. J. 262 (2015) 1–8. doi:10.1016/j.cej.2014.09.041.
[11] J. van Walsem, J. Roegiers, B. Modde, S. Lenaerts, S. Denys, Determination of intrinsic kinetic parameters in photocatalytic multi-tube reactors by combining the NTUm-method with radiation field modelling, Chem. Eng. J. 354 (2018) 1042–1049. doi:10.1016/j.cej.2018.08.010.
[12] R. Yang, Y.-P. Zhang, R.-Y. Zhao, An Improved Model for Analyzing the Performance of Photocatalytic Oxidation Reactors in Removing Volatile Organic Compounds and Its Application, J. Air Waste Manage. Assoc. 54 (2004) 1516–1524. doi:10.1080/10473289.2004.10471016.
[13] R. Yang, Y. Zhang, Q. Xu, J. Mo, A mass transfer based method for measuring the reaction coefficients of a photocatalyst, Atmos. Environ. 41 (2007) 1221–1229. doi:10.1016/j.atmosenv.2006.09.043.
[14] J. Roegiers, J. Van Walsem, S. Denys, CFD- and radiation field modeling of a gas phase photocatalytic multi-tube reactor, Chem. Eng. J. (2017) 1–33. doi:10.1016/J.CEJ.2018.01.047.
[15] J. van Walsem, S.W. Verbruggen, B. Modde, S. Lenaerts, S. Denys, CFD investigation of a multi-tube photocatalytic reactor in non-steady- state conditions, Chem. Eng. J. 304 (2016) 808–816. doi:10.1016/j.cej.2016.07.028.
[16] J. van Walsem, J. Roegiers, B. Modde, S. Lenaerts, S. Denys, Integration of a photocatalytic multi-tube reactor for indoor air purification in HVAC systems: a feasibility study, Environ. Sci. Pollut. Res. (2018). doi:10.1007/s11356-018-2017-z.
[17] P. Harb, L. Sivachandiran, V. Gaudion, F. Thevenet, N. Locoge, The 40 m3 Innovative experimental Room for INdoor Air studies (IRINA): Development and validations, Chem. Eng. J. 306 (2016) 568–578. doi:10.1016/j.cej.2016.07.102.
[18] P. Harb, N. Locoge, F. Thevenet, Emissions and treatment of VOCs emitted from wood-based construction materials : Impact on indoor air quality, Chem. Eng. J. 354 (2018) 641–652. doi:10.1016/j.cej.2018.08.085.
[19] S.W. Verbruggen, M. Keulemans, J. van Walsem, T. Tytgat, S. Lenaerts, S. Denys, CFD modeling of transient adsorption/desorption behavior in a gas phase photocatalytic fiber reactor, Chem. Eng. J. 292 (2016) 42–50. doi:10.1016/j.cej.2016.02.014.
[20] B. Ohtani, D. Li, R. Abe, What is Degussa (Evonik) P25 ? Crystalline composition analysis, reconstruction from isolated pure particles and photocatalytic activity test, J. Photochem. Photobiol. A Chem. 216 (2010) 179–182. doi:10.1016/j.jphotochem.2010.07.024.
[21] COMSOL Multiphysics® v. 5.2. COMSOL AB, CFD User's Guide, Stockholm, 2017.
[22] Y. Çengel, A.J. Ghajar, Heat and Mass Transfer: Fundamentals and Applications, 5th ed., McGraw-Hill, New York, 2014.
[23] A.H. Mamaghani, F. Haghighat, C.S. Lee, Photocatalytic oxidation technology for indoor environment air purification: The state-of-the-art, Appl. Catal. B Environ. 203 (2017) 247–269. doi:10.1016/j.apcatb.2016.10.037.
[24] J. Mo, Y. Zhang, Q. Xu, J.J. Lamson, R. Zhao, Photocatalytic purification of volatile organic compounds in indoor air: A literature review, Atmos. Environ. 43 (2009) 2229–2246. doi:10.1016/j.atmosenv.2009.01.034.
[25] S.B. Kim, S.C. Hong, Kinetic study for photocatalytic degradation of volatile organic compounds in air using thin film TiO2 photocatalyst, Appl. Catal. B Environ. 35 (2002) 305–315. doi:10.1016/S0926-3373(01)00274-0.
[26] Y. Chen, D.D. Dionysiou, TiO2 photocatalytic films on stainless steel: The role of Degussa P-25 in modified sol-gel methods, Appl. Catal. B Environ. 62 (2006) 255–264. doi:10.1016/j.apcatb.2005.07.017.
[27] B. Ohtani, Titania Photocatalysis beyond Recombination: A Critical Review, Catalysts. 3 (2013) 942–953. doi:10.3390/catal3040942.
[28] A. Fujishima, X. Zhang, D.A. Tryk, TiO2photocatalysis and related surface phenomena, Surf. Sci. Rep. 63 (2008) 515–582. doi:10.1016/j.surfrep.2008.10.001.

[29] A. Fujishima, T.N. Rao, D.A. Tryk, Titanium dioxide photocatalysis, J. Photochem. Photobiol. C Photochem. Rev. 1 (2000) 1–21. doi:10.1016/S1389-5567(00)00002-2.
[30] J.M. Herrmann, Heterogeneous photocatalysis: State of the art and present applications, Top. Catal. 34 (2005) 49–65. doi:10.1007/s11244-005-3788-2.
[31] Y. Çengel, J.M. Cimbala, R.H. Turner, Fundamentals of Thermal-Fluid Sciences, 4th ed., McGraw-Hill, New York, 2012.
[32] B. Kartheuser, N. Costarramone, T. Pigot, S. Lacombe, NORMACAT project: normalized closed chamber tests for evaluation of photocatalytic VOC treatment in indoor air and formaldehyde determination., Environ. Sci. Pollut. Res. Int. 19 (2012) 3763–71. doi:10.1007/s11356-012-0797-0.
[33] W. Chen, J.S. Zhang, UV-PCO device for indoor VOCs removal: Investigation on multiple compounds effect, Build. Environ. 43 (2008) 246–252. doi:10.1016/j.buildenv.2006.03.024.
[34] O. Debono, F. Thévenet, P. Gravejat, V. Héquet, C. Raillard, L. Le Coq, et al., Gas phase photocatalytic oxidation of decane at ppb levels: Removal kinetics, reaction intermediates and carbon mass balance, J. Photochem. Photobiol. A. 258 (2013) 17–29. doi:10.1016/j.jphotochem.2013.02.022.
[35] J. Mo, Y. Zhang, Q. Xu, Y. Zhu, J. Joaquin, R. Zhao, Determination and risk assessment of by-products resulting from photocatalytic oxidation of toluene, Appl. Catal. B Environ. 89 (2009) 570–576. doi:10.1016/j.apcatb.2009.01.015.
[36] J. Shang, Y. Du, Z. Xu, Kinetics of gas-phase photocatalytic oxidation of heptane over TiO2, React. Kinet. Catal. Lett. 75 (2002) 259–265. doi:10.1023/A:1015294811994.